Biochimica et Biophysica Acta 1842 (2014) 1668–1680

Contents lists available at ScienceDirect

Biochimica et Biophysica Acta

journal homepage: www.elsevier.com/locate/bbadis

AMPK-α1 functions downstream of oxidative stress to mediate neuronal atrophy in Huntington's disease

Tz-Chuen Ju [a], Hui-Mei Chen [a], Yu-Chen Chen [a,b], Ching-Pang Chang [b], Chen Chang [a], Yijuang Chern [a,b,*]

[a] Institute of Biomedical Sciences, Academic Sinica, Taipei 115, Taiwan
[b] Institute of Neuroscience, National Yang-Ming University, Taipei 112, Taiwan

ARTICLE INFO

Article history:
Received 13 December 2013
Received in revised form 27 May 2014
Accepted 9 June 2014
Available online 16 June 2014

Keywords:
AMP-activated protein kinase (AMPK)
Huntington's disease (HD)
Reactive oxygen species (ROS)
N-acetyl-L-cysteine (NAC)

ABSTRACT

Huntington's disease (HD) is an autosomal dominant neurological disorder that is induced by a CAG trinucleotide expansion in exon 1 of the *Huntingtin* (*HTT*) gene. We previously reported that the abnormal activation of an important energy sensor, AMP-activated protein kinase α1 (AMPK-α1), occurs in the brains of mice and patients with HD, which suggests that this abnormal activation may contribute to neuronal degeneration in HD. In the present study, we demonstrated that the elevated oxidative stress that was evoked by a polyQ-expanded mutant HTT (mHTT) caused the abnormal activation of AMPK-α1 and, subsequently, resulted in neurotoxicity in a striatal progenitor cell line (ST*Hdh*^{Q109}) and in the striatum of a transgenic mouse model of HD (R6/2). The systematic administration of an antioxidant (*N*-acetyl-cysteine, NAC) to R6/2 mice suppressed the activation of AMPK-α1, reduced neuronal toxicity, which was assessed by the activation of caspases, increased neuronal density, ameliorated ventricle enlargement, and improved motor dysfunction. This beneficial effect of NAC in vivo appears to be direct because NAC also reduced the activation of AMPK-α1 and the death of ST*Hdh*^{Q109} cells upon elevated oxidative stress. Moreover, the activation of AMPK enhanced the level of oxidative stress in ST*Hdh*^{Q109} cells, in primary neurons of R6/2 mice, and in the striatum of two different HD mouse models (R6/2 and *Hdh*$^{150Q/+}$), whereas the inhibition of AMPK reduced the level of oxidative stress. Collectively, our findings suggest that positive feedback regulation between the elevated oxidative stress and the activation of AMPK-α1 contributes to the progression of HD.

1. Introduction

Huntington's disease (HD) is an autosomal dominant neurodegenerative disease that is caused by a CAG trinucleotide expansion in exon 1 of the *Huntingtin* (*HTT*) gene, which is located on chromosome 4 (4p63). When the number of CAG repeats is higher than 36, the resultant polyQ-expanded mutant HTT (mHTT) protein is prone to aggregate formation, compromises the activity of proteasomes, dysregulates the transcription machinery (e.g., the suppression of the expression of BDNF and PGC-1α), impairs synaptic functions, elevates oxidative stress, degenerates axons, and eventually leads to neuronal atrophy and loss [1–5].

Elevated oxidative stress has been widely observed in neurodegenerative diseases, including HD, and is believed to play a critical role in HD pathogenesis. Specifically, high oxidative stress in HD is associated with proteasome malfunction, which acerbates aggregate formation, somatic CAG expansion in neurons [6], cell death [7], and the deficiency of the mitochondrial complex IV. Furthermore, mHTT inclusions appear to be the production source of reactive oxygen species (ROS) because a significant amount of oxidized proteins was detected in partially purified mHTT aggregates [8]. It is not surprising to find that the onset and progression of HD correlate well with the level of ROS in both mice and patients with HD [9–11]. Several antioxidants (such as green tea, coenzyme Q10, creatine, and BN82451) were used as treatment in animal models of HD and produced beneficial effects, including increased survival, improved motor functions, reduced brain atrophy and ventricular enlargement, and fewer intranuclear inclusions [12–14].

The AMP-activated protein kinase (AMPK) is a key energy sensor, which is important in maintaining energy homeostasis [15]. AMPK consists of three subunits (α, β, and γ) and is activated via the phosphorylation of the threonine residue 172 (Thr^{172}) of the α subunit. Several kinases are known to regulate the activity of AMPK, including

Abbreviations: 3D, three-dimensional; ACC, acety-CoA carboxylase; AD, Alzheimer's disease; AICAR, aminoimidazole carboxamide riboside; AMPK, AMP-activated protein kinase; ALS, amyotrophic lateral sclerosis; ATM, ataxia telangiectasia mutated; CaMKII, Ca^{2+}/calmodulin-dependent protein kinase II; CaMKK, calmodulin-dependent protein kinase kinase; CC, compound C; HD, Huntington's disease; *Htt*, Huntingtin; mHtt, mutant Htt; LKB1, liver kinase B1; MRI, magnetic resonance imaging; NES, nuclear export signal; NLS, nuclear localization signal; PD, Parkinson's disease; PGC-1α, peroxisome proliferator-activated receptor gamma co-activator 1α; PKA, cAMP-dependent kinase; polyQ, polyglutamine; TAK1, TGF-β-activated kinase; VBR, ventricle-to-brain ratio; WT, wild-type

* Corresponding author at: Institute of Biomedical Sciences, Academia Sinica, Nankang, Taipei 115, Taiwan. Tel.: +886 2 26523913; fax: +886 2 27829143.
E-mail address: bmychern@ibms.sinica.edu.tw (Y. Chern).

http://dx.doi.org/10.1016/j.bbadis.2014.06.012
0925-4439/

the calmodulin-dependent protein kinase kinase (CaMKK), liver kinase B1 (LKB1), TGF-β-activated kinase 1 (TAK1), cAMP-dependent kinase (PKA), ataxia telangiectasia mutated kinase (ATM), and Ca^{2+}/calmodulin-dependent protein kinase II (CaMKII) [16–21]. In the brain, AMPK plays a critical role in the regulation of food intake in hypothalamic neurons [22]. The importance of AMPK in neurodegenerative diseases (including HD, Alzheimer's disease, Parkinson's disease, and amyotrophic lateral sclerosis) has also been actively investigated [21,23–25].

The interplays between AMPK and ROS are complex. In some cells, AMPK is a downstream target of ROS. For example, oxidative stress selectively activates AMPK-α1, which stimulates glucose transport in skeletal muscle [26] and protects a rat dental pulp cell line (RPC-C2A) from damage that was caused by ROS [27]. However, AMPK was reported to exert anti-apoptotic effects through the suppression of ROS in other types of cells [28]. Specifically, the activation of AMPK was shown to reduce oxidative stress by modulating the level or activity of NAD(P)H oxidase, inducible nitric oxide synthase, cyclooxygenase-2, manganese superoxide dismutase, or uncoupling protein 2 [29]. We previously reported that, in striatal neurons of HD mice, AMPK-α1 is abnormally activated by mHTT via a CaMKII-dependent pathway and exerts a detrimental effect on neuronal survival via the suppression of the functions of two pro-survival proteins (i.e., CREB, Bcl2) [21]. The role of the interaction between AMPK-α1 and ROS in HD pathogenesis has not been previously characterized. In the present study, we demonstrated that elevated oxidative stress in the striatum is an important upstream positive regulator of AMPK-α1, which promotes mHTT aggregation and enhances the mHTT-mediated neuronal atrophy. Our data also suggest that positive feedback regulation between the activation of AMPK-α1 and the formation of ROS exists in striatal progenitor cell lines and primary neurons. Most importantly, chronic treatment with a ROS scavenger (*N*-acetyl-L-cysteine, NAC) ameliorated the detrimental effects of AMPK and protected striatal neurons from neuronal degeneration in HD.

2. Materials and methods

2.1. Animals and AICAR administration

R6/2 mice (B6CBA-Tg(HDexon1)62Gpb/1J) were originally obtained from Jackson Laboratories (Bar Harbor, ME, USA) [30]. The number of CAG repeats of R6/2 mice that were used in this study was 222 ± 5 (mean ± SEM). Animals were maintained on a 12-h light/dark cycle at the Institute of Biomedical Sciences Animal Care Facility. To activate AMPK in vivo, mice were subcutaneously administered AICAR (3 μg/animal/day) or saline into the striatum for 1 day via osmotic minipumps (ALZET, Cupertino, CA, USA). The AP and ML coordinates were 0.5 and ±2 mm relative to the bregma, respectively. The dorsoventral coordinates were −3, −2.7, and −2.4 mm relative to the bregma.

The knock-in *Hdh*^{150Q} mice (B6.129P2-*Hdh*tm2Detl/J) were initially obtained from Jackson Laboratories [31]. These mice harbor either one or two copies of mutant *HTT* containing 150 glutamine repeats (designated *Hdh*$^{150Q/+}$ and *Hdh*$^{150Q/150Q}$, respectively).

All animal experimental protocols were approved by the Academia Sinica Institutional Animal Care and Utilization Committee (Taipei, Taiwan).

2.2. Cell cultures and primary neuronal cultures

The striatal progenitor ST*Hdh*^{Q7} and ST*Hdh*^{Q109} cell lines, which were developed from wild-type mice and *Hdh*^{150Q} knock-in mice, respectively, were generous gifts from Dr. E. Cattaneo (University of Milano, Italy) [32]. These cells were maintained in an incubation chamber, which was gassed with 5% CO_2 at 33 °C. Cells were transfected using Lipofectamine 2000 (Invitrogen Corporation, Carlsbad, CA, USA) for 48 h according to the manufacturer's protocol.

Primary neuronal cultures were isolated from R6/2 mice and their littermate controls at embryonic day 18 (E18). Briefly, embryo cortices, hippocampus, and striatum were dissected and incubated in 0.05% trypsin-EDTA (Invitrogen, Grand Island, NY, USA) at 37 °C for 10 min. Trypsin activity was neutralized with fetal bovine serum (FBS). The digested tissue mixture was dissociated by gentle pipetting in modified Eagle's medium (MEM) containing 5% FBS, 1% insulin–transferrin–selenium supplement, 5% horse serum, 0.6% glucose, and 0.5 mM L-glutamine. Cells were plated onto poly-L-lysine-coated cover slips. After a 3 h-incubation, MEM was replaced with Neurobasal medium supplemented with 2% B27 (Invitrogen, San Diego, CA, USA), 12.5 mM glutamate, and 0.5 mM L-glutamine. Cells were maintained in an incubation chamber supplied with 5% CO_2/95% air at 37 °C.

2.3. Measurement of ROS

Cellular ROS contents were measured using the fluorescent probe 2,7-dichlorodihydrofluorescein diacetate (H_2DCFDA; Molecular Probes, Inc., Eugene, Oregon, USA). Briefly, cells were incubated with H_2DCFDA (50 μM) for 30 min at 33 °C in normal culture medium. Cells were washed 3 times in Locke's buffer (154 mM NaCl, 5.6 mM KCl, 2.3 mM CaCl2, 1 mM $MgCl_2$, 3.6 mM $NaHCO_3$, 15 mM Hepes, and 10 mM D-glucose, pH 7.3), lysed in Tris-EDTA buffer (10 mM Tris–HCl, 1 mM disodium EDTA, pH 8.0) containing 0.2% Triton X-100 for 10 min, and centrifuged at 15,000 *g* for 5 min at 4 °C. The cytoplasmic fraction was collected for the quantification of fluorescence intensity (Excitation/Emission: 488 nm/510 nm) by a fluorescence plate reader (Fluoroskan Ascent; Thermo Electron Corporation, Woburn, MA, USA).

To detect ROS in primary neurons, cells were incubated with the CellROX™ Deep Red Reagent (5 μM; Molecular Probes, Inc., Eugene, Oregon, USA) and Hoechst 33342 (1 μg/mL) for 30 min at 33 °C in normal culture medium. Cells were washed three times with PBS. Images were acquired using a laser confocal microscope (CellROX™ Deep Red Reagent: excitation/emission, 640 nm/665 nm; LSM780, Carl Zeiss MicroImaging).

The ROS level in brain tissues was measured using the OxiSelect™ In Vitro ROS/RNS Assay Kit (Cell Biolabs, Inc., San Diego, CA, USA). Briefly, tissue lysates (10 μL) were incubated with the catalyst (10 μL) in a 96-well plate for 5 min at room temperature (RT), followed by the addition of DCFH solution (100 μL) for a 30-min incubation at RT in the dark. Fluorescence was detected using a fluorescence plate reader (excitation/emission, 480 nm/530 nm).

To measure ROS in the brain, mice were intravenously injected with dihydroethidium (DHE, Invitrogen, Carlsbad, CA, USA; 0.5 mg per mouse) the day before harvesting [33]. Brain tissues were harvested to analyze ROS production using an IVIS spectrum imaging system (IVIS 200; Xenogen, CA, USA) with a fluorescence filter (Excitation: 500–550 nm, Emission: 575–650 nm). Data analyses were performed using the software Living Image (Xenogen).

2.4. Constructs

The mouse AMPK-α1 was amplified from a mouse brain cDNA by PCR and subcloned into pcDNA3.1 (Invitrogen, Carlsbad, CA, USA). The preparation of the dominant positive and negative mutants of AMPK-α1 (AMPK-α1-172$^{T/D}$, AMPK-α1-172$^{T/A}$, AMPK-α1-172$^{T/D}$-NLS/NES:YFP, AMPK-α1-172$^{T/A}$-NLS:YFP) was described previously.

2.5. Cell death assays

ST*Hdh*^{Q7} and ST*Hdh*^{Q109} cell death was quantified by the MTT reduction assay and by a flow cytometric analysis. For the MTT reduction assay, 3-[4,5-dimethylthiazol-2-yl]-2,5-diphenyltetrazolium bromide (MTT) was dissolved in dimethyl sulfoxide (DMSO) at 50 mg/ml as a

100-fold stock solution. At the end of experiments, cells were incubated in culture medium with 0.5 mg/ml MTT at 37 °C for 2 h. The culture medium was then replaced with DMSO to dissolve the MTT formazan precipitates, which was followed by the measurement of the absorbance at 570 nm using a microplate reader (OPTImax tunable plate reader, Molecular Device, Sunnyvale, CA, USA).

Apoptotic analyses of ST*Hdh*^{Q7} and ST*Hdh*^{Q109} cells by flow cytometry were conducted by staining cells using propidium iodide (PI) and were analyzed by a flow cytometer (BD Biosciences, San Jose, CA, USA). Briefly, cells were rinsed with ice-cold phosphate-buffered saline (PBS) at the end of drug treatment, fixed with ethanol (70%) at −20 °C for 1 h, and rehydrated using ice-cold PBS. PI (50 μg/ml) was then added into cell suspension to stain cells before subjecting them to the flow cytometric analysis. Cells existing in the sub-G1 phase were considered apoptotic cells. At least 10,000 gated cells were counted for each sample. The data were analyzed using the CellQuest™ software (BD Biosciences, San Jose, CA, USA).

For in vivo cell death assays, the SR-FLIVO™ in vivo apoptosis assay kit (Immunochemistry Technologies, LLC, Bloomington, MN, USA) was employed [34]. In brief, SR-FLIVO™ was intravenously injected into the lateral tail vein of each mouse and allowed to circulate in the animal for 60 min. Mouse brains were then perfused with 4% paraformaldehyde in 0.1 M phosphate buffer (PB, pH 7.4) as described above. Coronal serial sections (20 μm) were used to analyze the activation of caspases by detecting the signal of SR-FLIVO™ using a laser confocal microscope (LSM780) with excitation at 565 nm and emission at 600 nm. The quantitation of active caspases was analyzed by a MetaMorph imaging system (Universal Imaging, Westchester, PA, USA).

2.6. SDS-polyacrylamide gel electrophoresis (PAGE) and western blotting

Cellular proteins were extracted in TNE buffer [50 mM Tris–HCl (pH 7.4), 100 mM NaCl, 0.1 mM EDTA and 1% Triton X-100]. Proteins were electrophoretically fractionated through 10% and 15% PAGE and then electrotransferred onto PVDF membranes (Millipore, Bedford, MA, USA) for Western blot analyses. Dilutions of the primary antibodies that were used in the present study are listed below: anti-phospho-AMPKα^{T172} (1:1000, Cell Signaling Technology, Danvers, MA, USA), anti-AMPK-α1 (1:1000, Abcam Cambridge, MA, USA), anti-phospho-CaMKII^{T286} (1:1000; Abcam), anti-CaMKII (1:1000; Abcam) and anti-Actin (1:5000; Santa Cruz Biotechnology, Inc., Santa Cruz, CA, USA). Immunoreactive signals on Western blots were detected using an ECL detection system (PerkinElmer Life and Analytical Sciences, Boston, MA, USA).

2.7. Immunohistochemical staining

Immunohistochemical staining was performed as previously described [21]. For brain sections, mice were fixed by perfusion with 4% paraformaldehyde in phosphate buffer (PB, 0.1 M sodium phosphate pH 7.4). After perfusion, the brain tissues were removed and post-fixed with 4% paraformaldehyde/0.1 M PB overnight, immersed in 30% sucrose in 0.1 M PB for several days, and frozen at −80 °C. The brain sections (20 μm) were incubated with the desired primary antibodies in PBS containing 5% normal goat serum at 4 °C overnight and were then incubated with the corresponding secondary antibody for 2 h at room temperature. Dilutions of the primary antibodies that were used in the present study are listed below: anti-phospho-AMPKα^{T172} (1:100, Cell Signaling Technology, Danvers, MA, USA), anti-AMPKα1 (1:200, Cell Signaling Technology, Danvers, MA, USA), and anti-NeuN (1:1000, NeuN, Millipore, Bedford, MA, USA). The nuclei were stained with Hoechst 33258. The immunostaining pattern was visualized using a laser confocal microscope (LSM780, Carl Zeiss MicroImaging).

The quantitation of immunofluorescence signals in primary neurons was performed on a laser confocal microscope using 40× oil-immersion objective lenses (LSM780, Carl Zeiss MicroImaging) and analyzed using the MetaMorph imaging system (Universal Imaging, Westchester, PA, USA). The fluorochromes used in the present study were Alexa Fluor 405, Alexa Fluor 488, and Alexa Fluor 633. At least 50 cells from each animal were counted and analyzed.

2.8. Micromagnetic resonance imaging (μMRI) analysis

Three-dimensional (3D) and whole-brain ventricle images of mice were evaluated using a Bruker PharmaScan (7T) scanner (Madison, WI, USA) as described previously [21]. The ventricle-to-brain ratio (VBR) was calculated by dividing the value of the ventricle by that of the entire brain.

2.9. Filter retardation assay

Brain tissues were suspended and homogenized in ice-cold TNE buffer (50 mM Tris–HCl (pH 7.4), 100 mM NaCl, 0.1 mM EDTA and 1% Triton X-100), mixed with 2% SDS. Samples were first passed through OE66 membrane filters (0.2 mm pore size; Whatman Schleicher and Schuell, Middlesex, UK) in a slot-blot manifold (Bio-Rad, Irvine, CA, USA). The membrane filters were blocked with 5% skim milk in TBST and incubated overnight with an anti-Htt antibody (1:500; Millipore Bioscience Research reagents, Temecula, CA, USA) at 4 °C, followed by 1 h incubation with the secondary antibody at room temperature. Immunoreactive signals were detected using an ECL detection system and were recorded using Kodak XAR-5 films.

2.10. Statistical analysis

Results were expressed as means ± SEM of triplicate samples. Each experiment was repeated at least three times to confirm the reproducibility of findings. Multiple groups were analyzed by one-way analysis of variance (ANOVA) followed by a post hoc Student–Newman–Keuls test. Differences were considered statistically significant if the *P* value was less than 0.05.

3. Results

3.1. Elevated oxidative stress in the brain of HD mice contributes to the activation of AMPK-α1 in striatal neurons

AMPK is known to be regulated by multiple upstream regulators. We set out to determine whether, in addition to the CaMKII-mediated pathway, additional pathway(s) are involved in the activation of AMPK-α1 in striatal neurons of HD mice. We are particularly interested in oxidative stress because it is a well-recognized contributor to HD pathogenesis [10,21]. In addition, CaMKII is known to mediate the actions of H_2O_2 in controlling signaling pathways, including ERK1/2, PKB, and IGF-1R, in several cell types [35,36]. We first showed that the overall ROS level in the brain of a transgenic mouse model (R6/2, [30]) at the age of 12 weeks was significantly higher than that of wildtype mice (Fig. 1A). To measure the ROS level in vivo, mice were intravenously injected with a fluorescent dye (dihydroethidium, DHE; 0.5 mg per mouse) that is sensitive to superoxide production. The ROS level in the brain was measured using an in vivo IVIS imaging system. Our findings are consistent with several earlier studies, which showed higher levels of ROS and/or more severe oxidative damage in brains of HD mice [9]. Daily treatment with a ROS chelator (NAC, 250 mg/kg of body weight, intraperitoneal injection) for 5 weeks from the age of 7 weeks markedly reduced the level of ROS in the brain (Fig. 1A).

Similar to what was found in R6/2 mice, the total ROS level in the striatum of HD knock-in mice (*Hdh*$^{150Q/150Q}$, [31]), which was measured using an in vitro ROS assay, was higher than that of their littermate controls (Fig. S1). We next determined the ROS level in striatal progenitor cells, which were derived from wild-type mice (ST*Hdh*^{Q7}) or knock-in mice (ST*Hdh*^{Q109}) that express HTT proteins harboring 7 and 109 copies of the CAG repeat, respectively. The cellular level of ROS was assessed

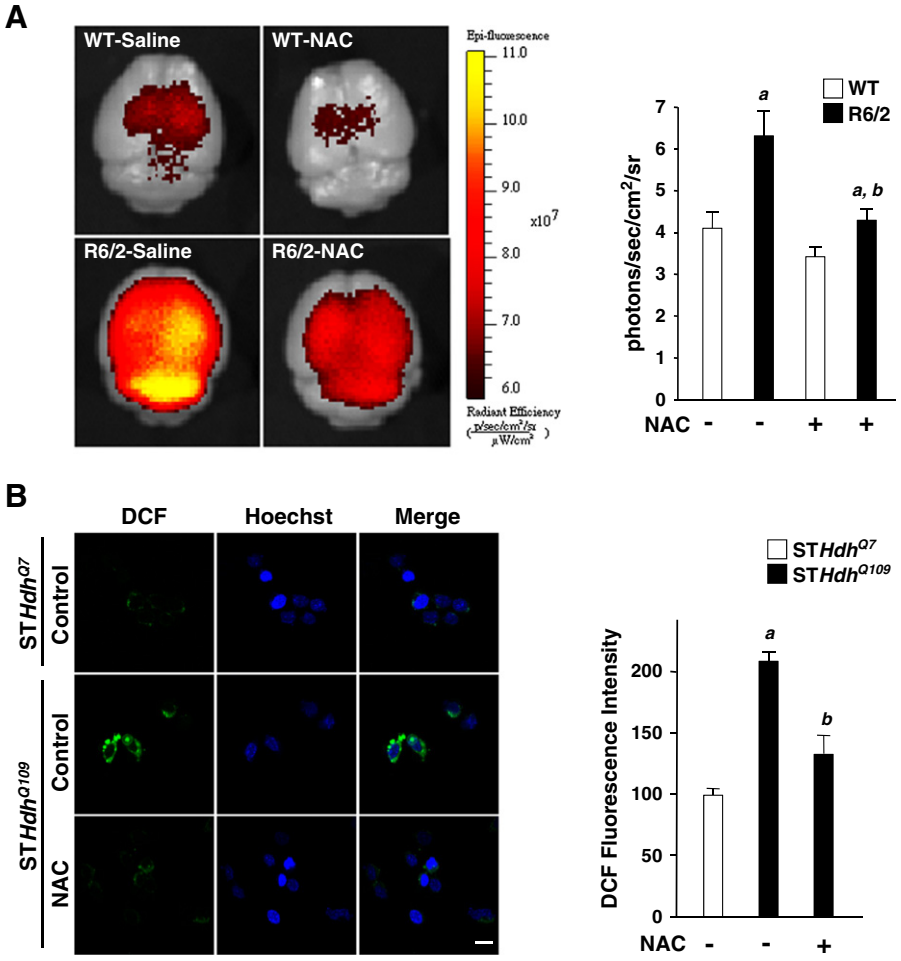

Fig. 1. Expression of polyQ-expanded mutant Huntingtin enhances the level of reactive oxygen species (ROS). (A) Mice were treated daily with an antioxidant (*N*-acetyl-L-cysteine, NAC; 250 mg/kg of body weight, intraperitoneal injection) or vehicle for 5 weeks from the age of 7 weeks. Wild-type mice [saline-treated WT mice ($n = 5$), saline-treated R6/2 mice ($n = 6$), NAC-treated WT mice ($n = 5$), and NAC-treated R6/2 mice ($n = 6$)] that were 12-weeks old were intravenously injected with a ROS sensor (dihydroethidium, DHE; 0.5 mg per mouse). One day post-injection, brain tissues were harvested to analyze the ROS levels using an IVIS® spectrum imaging system. The histograms show the florescence intensity of DHE. The pseudo colors represent photons/sec/cm^2/Sr. The data are presented as the mean ± SEM. [a]$p < 0.05$, between WT and R6/2 mice. [b]$p < 0.05$ vs. R6/2-saline-treated mice. (B) To measure cellular ROS levels, cells were incubated with H_2DCFDA (50 μM) for 30 min, followed by treatment with NAC (5 mM) for 24 h. The fluorescence intensity was quantified as described in the Materials and methods section. The data are presented as the mean ± SEM from three independent experiments. [a]$p < 0.05$ specific comparison between ST*Hdh*^{Q7} and ST*Hdh*^{Q109} cells. [b]$p < 0.05$ vs. untreated cells. Sale bars are 10 μm.

using a fluorescent probe (dihydrodichlorofluorescein diacetate, H_2DCF-DA). When compared with ST*Hdh*^{Q7} cells, elevated ROS levels were detected in the ST*Hdh*^{Q109} cells (Fig. 1B). As expected, NAC (5 mM) significantly reduced the ROS levels in ST*Hdh*^{Q109} cells.

To assess the influence of elevated ROS levels, we examined the effect of chronic treatment with NAC on disease progression in R6/2 mice. As shown in Fig. 2, chronic NAC treatment significantly ameliorated the striatal atrophy of R6/2 mice, which was determined by in vivo three-dimensional (3D) magnetic resonance imaging (MRI, Fig. 2A), enhanced the number of striatal neurons, which was assessed by immunocytochemical staining (Fig. 2B), and reduced striatal toxicity, which was determined by the level of activated caspases using an in vivo fluorescent dye that recognizes activated caspase (SR-FLIVO™) (Fig. 2C). Consistent with the improved neuronal survival in the striatum, NAC also markedly enhanced the impaired motor function of R6/2 mice, which was evaluated by rotarod performance (Fig. 2D), and reduced aggregate formation in the striatum (Fig. 2E). These findings are consistent with previous findings, which showed that antioxidant reagents produced beneficial effects on HD progression [12–14,37,38], and support the hypothesis that elevated oxidative stress plays a key pathogenic role in HD.

To determine whether AMPK is involved in the detrimental function of ROS, we first evaluated whether the reduction of ROS by NAC affected the activation of AMPK in R6/2 mice. As shown in Fig. 3, chronic treatment with NAC significantly reduced the phosphorylation (activation) level of AMPK at Thr^{172} (AMPKα-p^{172}, Fig. 3A). We previously demonstrated that AMPK regulated the expression of a survival factor, Bcl2 [39]. As shown in Fig. 3B, chronic treatment with NAC significantly enhanced the level of Bcl2 in R6/2 mice. Moreover, NAC also reduced the expression of AMPKα-p^{172} and AMPK-α1 in striatal nuclei of 12-week-old R6/2 mice (Fig. 3C, D). Given that the activation of AMPK-α1 in striatal neurons leads to the enrichment of AMPK-α1 in their nuclei [39], the above finding suggests that elevated ROS caused the activation of AMPK-α1 in the striatum. Consistent with the above hypothesis, we found that NAC, as well as an inhibitor (Compound C, CC) of AMPK, reduced the elevated level of AMPKα-p^{172} in ST*Hdh*^{Q109} cells (Fig. 3E). The level of AMPKα-p^{172} in ST*Hdh*^{Q109} cells was higher than that in ST*Hdh*^{Q7} cells, which was consistent with earlier reports [39]. In addition, the elevation of the ROS level in ST*Hdh*^{Q109} and ST*Hdh*^{Q109} by H_2O_2 dose-dependently increased the level of AMPKα-p^{172} (Fig. 3F, Supplementary Fig. S2, respectively). These data collectively support our hypothesis that ROS might mediate, at least partially, the

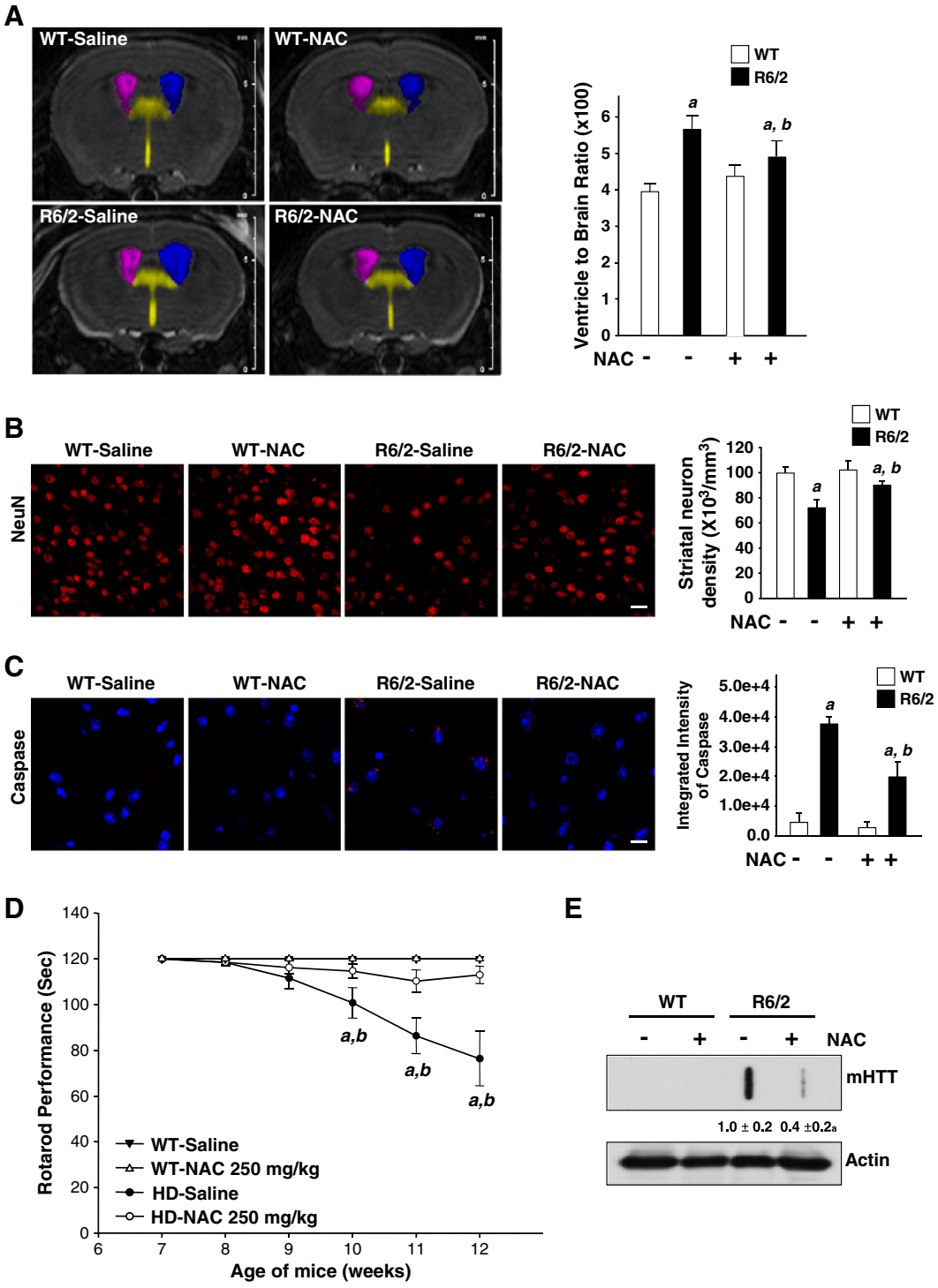

Fig. 2. A scavenger (*N*-acetyl-L-cysteine, NAC) of reactive oxygen species (ROS) markedly reduced the disease progression of a transgenic mouse model (R6/2) of HD. (A) Mice were treated daily with NAC (250 mg/kg of body weight, intraperitoneal injection) or vehicle for 5 weeks from the age of 7 weeks. Representative 3D brain images from vehicle-treated WT mice ($n = 6$), saline-treated R6/2 mice ($n = 7$), NAC-treated WT mice ($n = 5$), and NAC-treated R6/2 mice ($n = 7$). The ventricle-to-brain ratio (VBR) values were illustrated in the right panel. The data are presented as the mean ± SEM. $^{a}p < 0.05$, between WT and R6/2 mice. $^{b}p < 0.05$ vs. saline-treated mice. (B, C) The numbers of neurons (identified by the expression of NeuN; red, B) and the level of active caspases (red, C) in the striatum of the indicated mice [saline-treated WT mice ($n = 6$), saline-treated R6/2 mice ($n = 6$), NAC-treated WT mice ($n = 6$), and NAC-treated R6/2 mice ($n = 6$)] were quantified. Nuclei were stained with Hoechst (blue). The histograms show the number of striatal neurons (B) and the integrated intensity of active caspases (C). At least 600 cells from each animal were counted. The data are presented as the mean ± SEM. $^{a}p < 0.05$, between WT and R6/2 mice. $^{b}p < 0.05$ vs. saline-treated R6/2 mice. Scale bars, 20 μm. (D) Rotarod performance ($n =$ 10–12 for each condition) was determined. The data are presented as the mean ± SEM. $^{a}p < 0.05$, between WT and R6/2 mice. $^{b}p < 0.05$ vs. NAC-treated R6/2 mice. (E) The level of mHTT aggregates in striatal lysates was analyzed by a filter retardation assay. Insoluble aggregates that were retained on the filters were detected using an anti-HTT antibody. The data are presented as the mean ± SEM from three independent experiments. $^{a}p < 0.05$ vs. saline-treated R6/2 mice.

activation of AMPK-α1 by mHTT. Note that chronic NAC treatment did not reduce the autophosphorylation level of CaMKII, which reflected the activity of CaMKII, in the striatum of R6/2 mice (Supplementary Fig. S3). Therefore, we conclude that ROS did not activate CaMKII in the striatum of HD mice and that CaMKII was not involved in the activation of AMPK by H_2O_2 in striatal neurons of HD mice.

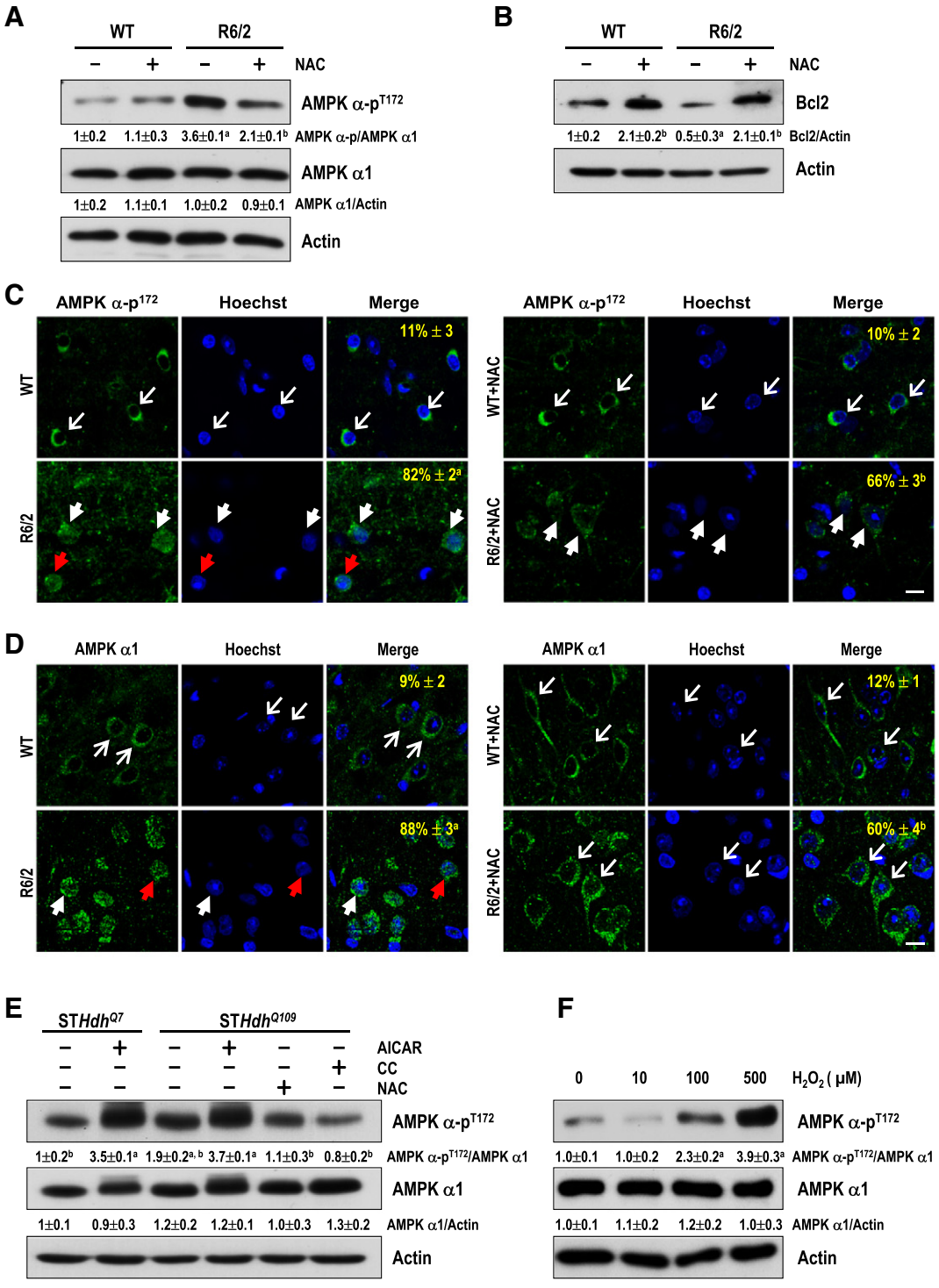

Fig. 3. The elevated reactive oxygen species (ROS) evoked abnormal activation of AMPK-α1 in the presence of polyQ-expanded mutant Huntingtin (HTT) in striatal cells. (A–D) Mice were treated daily with a ROS scavenger (*N*-acetyl-L-cysteine, NAC; 250 mg/kg of body weight, intraperitoneal injection) or vehicle for 5 weeks from the age of 7 weeks. (A, B) Striatal lysates were analyzed by Western blot analyses. The results were normalized to those results of actin. The data are presented as the mean ± SEM from three independent experiments. $^{a}p < 0.05$, between WT and R6/2 mice. $^{b}p < 0.05$ vs. saline-treated mice. The phosphorylation (activation) level of AMPK at Thr^{172} (AMPKα-p^{172}, C) and AMPK-α1 (D) in the striatum of the indicated animals ($n = 3$–6 for each condition) are shown. Nuclei were stained with Hoechst (blue). The numbers shown in the upper-right corners of the merged images are the percentage of cells expressing nuclear AMPKα-p^{172} or AMPK-α1 as indicated. Red arrows mark cells with AMPKα-p^{172} (C) or AMPK-α1 (D) only in nuclei. Thick arrows mark cells with AMPKα-p^{172} (C) or AMPK-α1 (D) existing in cytoplasmic and nuclei. Thin arrows mark cells expressing AMPKα-p^{172} (C) or AMPK-α1 (D) only in cytoplasmic regions as indicated. At least 200 cells from each animal were counted. The data are presented as the mean ± SEM. $^{a}p < 0.05$, between WT and R6/2 mice. $^{b}p < 0.05$ vs. saline-treated R6/2 mice. Scale bars, 20 μm. (E) Cells were treated with AICAR (1 mM), NAC (5 mM), or CC (10 μM) for 24 h. The data are presented as the mean ± SEM from three independent experiments. $^{a}p < 0.05$ vs. untreated STHdh^{Q7} cells. $^{b}p < 0.05$, vs. AICAR-treated cells. (F) STHdh^{Q109} cells were treated with H_2O_2 of the indicated concentration for 1 h. Total lysates were assessed by Western blot analyses. The results were normalized to those results of actin. The data are presented as the mean ± SEM from three independent experiments. $^{a}p < 0.05$ vs. untreated cells.

3.2. Positive feedback regulation between the activation of AMPK-α1 and the formation of ROS in striatal neurons

We next evaluated whether AMPK-α1 contributed to the enhanced ROS in striatal cells. Consistent with the image analyses that are shown in Fig. 1B the ROS level in ST*Hdh*^{Q109} cells was higher than that in ST*HdH*^{Q7} cells (Fig. 4A). As expected, NAC (5 mM) markedly reduced the elevated ROS levels in both ST*HdH*^{Q7} and ST*Hdh*^{Q109} cells. Moreover, an AMPK inhibitor (CC) suppressed the elevated ROS levels in ST*Hdh*^{Q109} cells, indicating that AMPK might regulate the elevation of oxidative stress. Consistent with this hypothesis, the activation of AMPK using AICAR dose-dependently enhanced cellular oxidative stress in ST*Hdh*^{Q7} and ST*Hdh*^{Q109} cells (Fig. 4B). Notably, a low dose of AICAR (0.1 mM) enhanced the level of ROS only in ST*Hdh*^{Q109} cells but not in the control ST*Hdh*^{Q7} cells, which suggests that mHTT might render striatal neurons more susceptible to the feedback regulation between AMPK and ROS (Fig. 4B). In addition, the exogenous expression of a wild-type or constitutively active mutant of AMPK-α1 (AMPK-α1-172$^{T/D}$) enhanced cellular oxidative stress in ST*Hdh*^{Q7} and ST*Hdh*^{Q109} cells (Fig. 4C). Conversely, the inhibition of AMPK using CC or a dominant negative mutant of AMPK (AMPK-α1-172$^{T/A}$) markedly reduced the elevated ROS levels that were evoked by H_2O_2 (Fig. 4C, D, E).

Consistent with the findings from ST*Hdh*^{Q109} cells (Figs. 3F and 4B), primary striatal neurons harvested from R6/2 mice had higher levels of AMPK activation and ROS than did WT striatal neurons (Fig. 5). Treatment with an AMPK activator (AICAR) caused not only the activation of AMPK (Fig. 5A and B), but also an enhancement of ROS (Fig. 5A and C). As was observed in Fig. 5, the elevation of ROS induced by H_2O_2 in the primary striatal neurons of R6/2 mice also led to an enhanced level of AMPK activation, which demonstrated the existence of a positive feedback regulation between ROS and AMPK activation. This positive loop was also observed in other types of primary neurons (including cortical and hippocampal neurons) collected from R6/2 mice (Supplementary Fig. S4).

Similar to the findings obtained in striatal progenitor cells and primary neurons, the activation of AMPK by AICAR in the striatum of R6/2 mice greatly enhanced the ROS level in the brain (Fig. 6A). In addition, the activation of AMPK in the striatum of *Hdh*$^{150Q/+}$ mice by intrastriatal injection of an activator of AMPK (AICAR) not only enhanced AMPK activation (as monitored by the expression of AMPK-α-P^{T172}) (Fig. 6B), but also increased the ROS level (as determined using an in vitro ROS assay) (Fig. 6C). These observations suggest that the activation of AMPK in the striatum of HD mice leads to an increase in ROS levels in vivo. Taken together, our data support the hypothesis that AMPK-α1 is not only a downstream target of ROS, but also positively regulates ROS production in striatal neurons that express mHTT.

3.3. Positive regulation between ROS and AMPK is critical for the survival of neurons that express mHTT

Consistent with the detrimental roles of ROS and AMPK in HD mice, we demonstrated that blocking ROS and AMPK using NAC and CC,

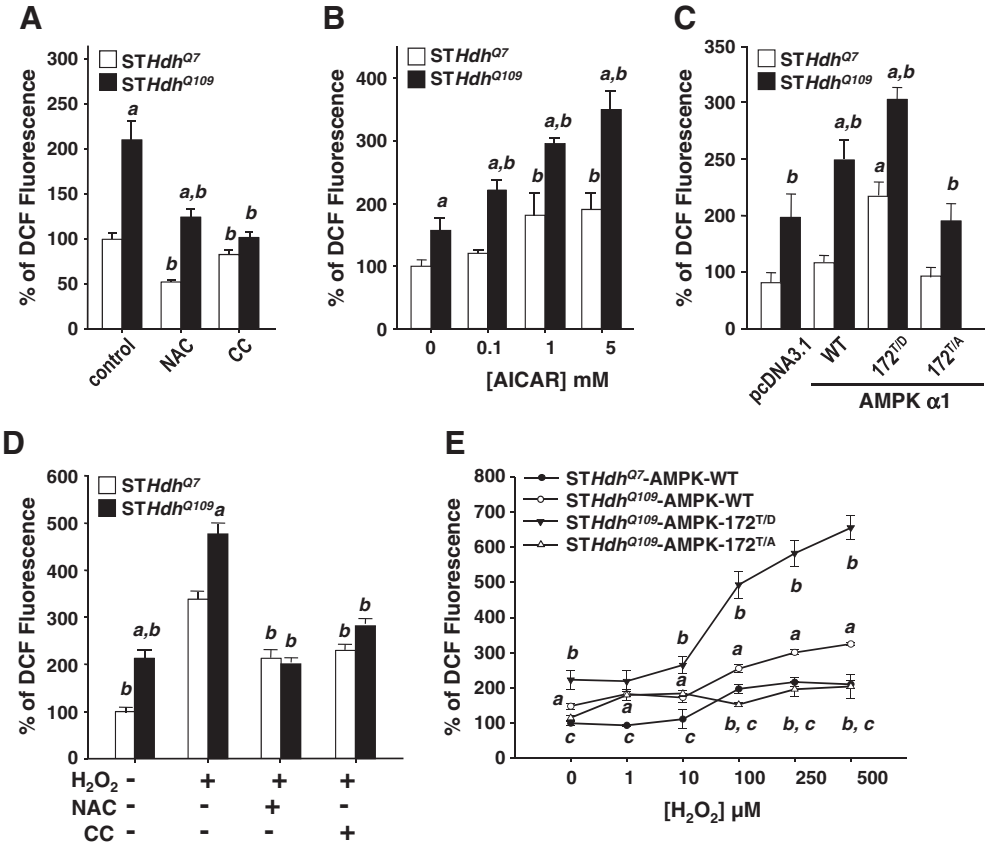

Fig. 4. Activation of AMPK-α1 promoted ROS production in striatal cells. (A–E) To measure cellular ROS, cells were incubated with H_2DCFDA (50 μM) for 30 min. (A) Cells were treated with NAC (5 mM) and an AMPK inhibitor (compound C, CC; 10 μM) for 6 h, and incubated with H_2DCFDA (50 μM) for 30 min. The data are presented as the mean ± SEM from three independent experiments. $^{a}p < 0.05$ specific comparison between ST*Hdh*^{Q7} and ST*Hdh*^{Q109} cells. $^{b}p < 0.05$ vs. untreated cells. (B) Cells were treated with AICAR at the indicated concentration for 1 h. The data are presented as the mean ± SEM from three independent experiments. $^{a}p < 0.05$, specific comparison between ST*Hdh*^{Q7} and ST*Hdh*^{Q109} cells. $^{b}p < 0.05$ vs. untreated cells. (C) ST*Hdh*^{Q7} and ST*Hdh*^{Q109} cells were transfected with the indicated cDNA for 48 h. The data are presented as the mean ± SEM from three independent experiments. $^{a}p < 0.05$ vs. cells transfected with the empty vector. $^{b}p < 0.05$, specific comparison between ST*Hdh*^{Q7} and ST*Hdh*^{Q109} cells. (D) Cells were treated with NAC (5 mM) or CC (10 μM) for 1 h, followed by a 30-min incubation with H_2O_2 (100 μM). The data are presented as the mean ± SEM from three independent experiments. $^{a}p < 0.05$, specific comparison between ST*Hdh*^{Q7} and ST*Hdh*^{Q109} cells. $^{b}p < 0.05$ vs. H_2O_2-treated cells. (E) Cells were transfected with the indicated construct for 48 h, and then treated with H_2O_2 for 1 h. The data are presented as the mean ± SEM from three independent experiments. $^{a}p < 0.05$, specific comparison between ST*Hdh*^{Q7} and ST*Hdh*^{Q109} cells. $^{b}p < 0.05$ vs. WT transfected cells. $^{c}p < 0.05$ vs. AMPK-172$^{T/D}$ transfected cells.

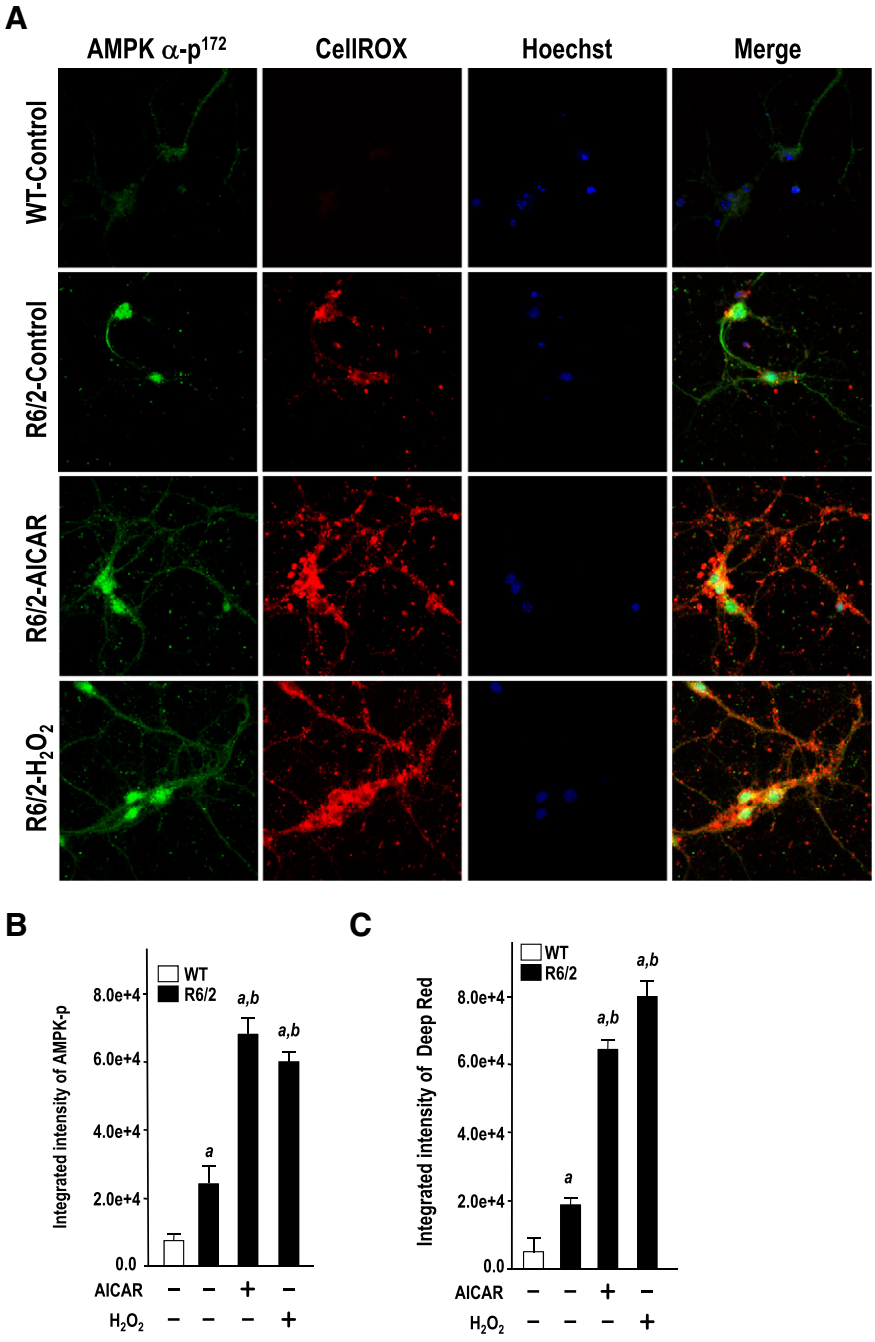

Fig. 5. Positive feedback regulation between reactive oxygen species (ROS) and AMPK in mutant Huntingtin (HTT)-expressing primary striatal neurons. (A–C) Cells were treated with or without the indicated reagents (1 mM AICAR for 24 h or 100 μM H_2O_2 for 1 h). To measure cellular ROS levels, neuronal cells were incubated with the CellROX™ Deep Red Reagent (red, 5 μM) for 30 min, followed by treatment with AICAR or H_2O_2. The levels of phosphorylation (activation) of AMPK at Thr^{172} (green, AMPKα-p^{172}) in the primary striatal neurons of the indicated animals ($n = 4$–6 for each condition) are shown. Nuclei were stained with Hoechst (blue). The fluorescence intensity was quantified as described in the Materials and methods section. Scale bars, 20 μm. At least 50 cells from each animal were counted. The histogram shows the fluorescence intensity of AMPKα-p^{172} (B) and CellROX™ Deep Red (C) in primary striatal neurons. The data are presented as the mean ± SE from three independent experiments. $^{a}p < 0.05$ between untreated WT and R6/2 mice; $^{b}p < 0.05$ vs untreated R6/2 mice.

respectively, enhanced the survival of ST*Hdh*^{Q109} cells upon abnormal AMPK activation (Fig. 7A, C) or elevated oxidative stress (Fig. 7B, D). Cell survival was determined using the MTT (Fig. 7A, B) and the flow cytometric assay (Fig. 7C, D). As shown in Fig. 7A and C, a ROS scavenger (NAC, 5 mM) blocked the death of ST*Hdh*^{Q109} cells that was caused by the activation of AMPK using AICAR (1 mM). Conversely, an AMPK inhibitor (CC, 10 μM) protected ST*Hdh*^{Q109} cells from the death that was triggered by elevated ROS (Fig. 7B, D). These observations support our hypothesis that positive feedback regulation between the activation of AMPK and the formation of ROS is critical for the survival of striatal neurons upon stresses.

4. Discussion

We previously demonstrated that AMPK-α1 is activated by a CaMKII-mediated pathway in striatal neurons of HD and that AMPK-α1 exerted a detrimental role in the progression of HD [21]. Because HD is a complex disease and because AMPK has multiple upstream regulators, in the present study, we investigated whether additional pathway(s) were involved in the regulation of AMPK-α1 in HD. Our results indicated that the expression of mHTT in a striatal progenitor cell line and in a transgenic mouse model of HD induces the accumulation of ROS, which, at least partially, mediates the activation of AMPK-α1

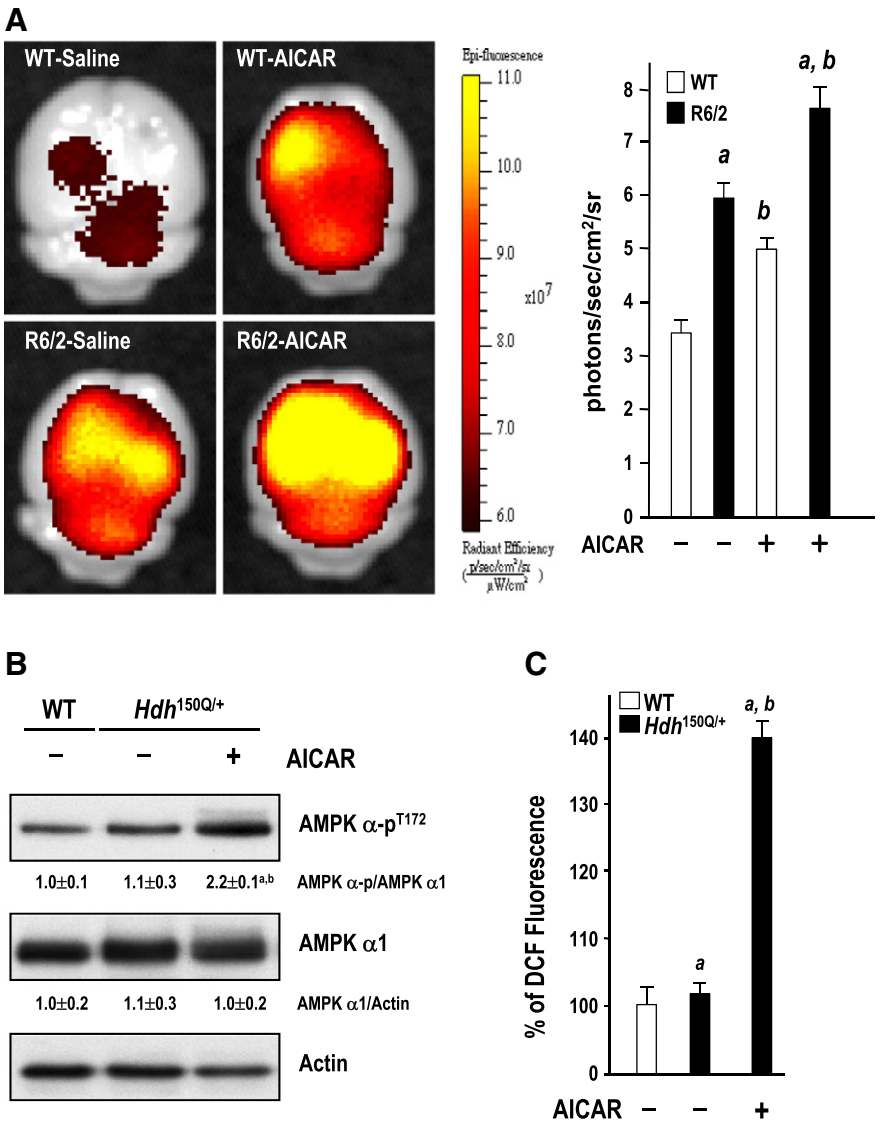

Fig. 6. Positive feedback regulation between reactive oxygen species (ROS) and AMPK in a transgenic mouse model (R6/2) and in a knock-in mouse model (*Hdh*^{150Q}) of HD. (A) Mice were treated with AICAR (10 μg per mouse) or saline for 1 day at the age of 12 weeks, followed by an intravenous injection of hydroethidine (DHE, 0.5 mg per mouse). One day postinjection, brain tissues were harvested to analyze ROS production using an IVIS spectrum imaging system. Brain images of mice (saline-treated WT mice ($n = 10$), saline-treated R6/2 mice ($n = 8$), AICAR-treated WT mice ($n = 9$), and AICAR-treated R6/2 mice ($n = 8$)) were used to determine the ROS level in the brain. The histograms show the fluorescence intensity of DHE. The pseudocolors represent photons/s/cm^2/Sr. The data are presented as the mean ± SEM. $^{a}p < 0.05$ between WT and R6/2 mice; $^{b}p < 0.05$ vs saline-treated mice. (B, C) Mice aged 22 months ($n = 3$–4 for each condition) were intrastriatally injected with AICAR (10 μg per mouse) or saline. One day postinjection, brain lysates were harvested to analyze the expression of AMPKα-p^{172} (B) or DCF fluorescence (C). The fluorescence intensity was quantified as described in the Materials and methods section. The data are presented as the mean ± SEM. $^{a}p < 0.05$ between WT and *Hdh*^{150Q} mice; $^{b}p < 0.05$ vs saline-treated *Hdh*^{150Q} mice.

(Figs. 2 and 3). Moreover, although ROS is capable of triggering multiple signaling pathways depending on the extent and duration of oxidative stress [40], the activation of AMPK by ROS is more commonly associated with high levels and/or long-term oxidative stresses [41,42]. The chronic treatment of HD mice with a blocker of ROS (NAC) not only reduced the activation and nuclear enrichment of AMPK-α1 but also rescued the levels of a survival signal (Bcl2), which was impaired by AMPK-α1 (Fig. 3). Our findings suggest that ROS is another damaging factor that functions upstream of AMPK-α1 in HD. It has been suggested that the initial cause of elevated ROS levels in HD patients at early stages may result from the mHTT-evoked abnormal trafficking of the neuronal glutamate transporter, whereas, at late stages, elevated ROS levels may be evoked by inferior mitochondrial functions [43–45].

Our data also showed that the activation of AMPK-α1 led to the increased production of ROS in a striatal progenitor cell line that expressed the full-length mHTT and in the striatum of two different mouse models of HD (Figs. 5–6). In addition to the suppression of CREB and Bcl2, in the present study, we showed that the overactivation of AMPK-α1 stimulates an additional harmful pathway that enhanced the mHTT-induced neurotoxicity. These findings suggest that positive feedback regulation between ROS and AMPK-α1 exists in striatal neurons of HD. Therefore, both NAC (an antioxidant) and CC (an inhibitor of AMPK) were neuroprotective in striatal neurons expressing mHTT (Figs. 2, 7). Therapeutic treatment(s) that prevent the vicious cycle between ROS formation and the activation of AMPK-α1 might disrupt this positive feedback loop and delay the progression of HD.

For HD and many other neurodegeneration diseases (including Alzheimer's Disease, AD; Parkinson's disease, PD; and amyotrophic lateral sclerosis, ALS), oxidative stress is one of the most harmful factors that exacerbate disease progression [46–48]. The glial cell-mediated increase of oxidative stress in the substantial nigra is generally believed to affect the onset and progression of PD [49]. The major disease-causing factor (the amyloid-β peptide) of AD is also known to induce the production of free radicals [50], whereas chronic treatment with NAC

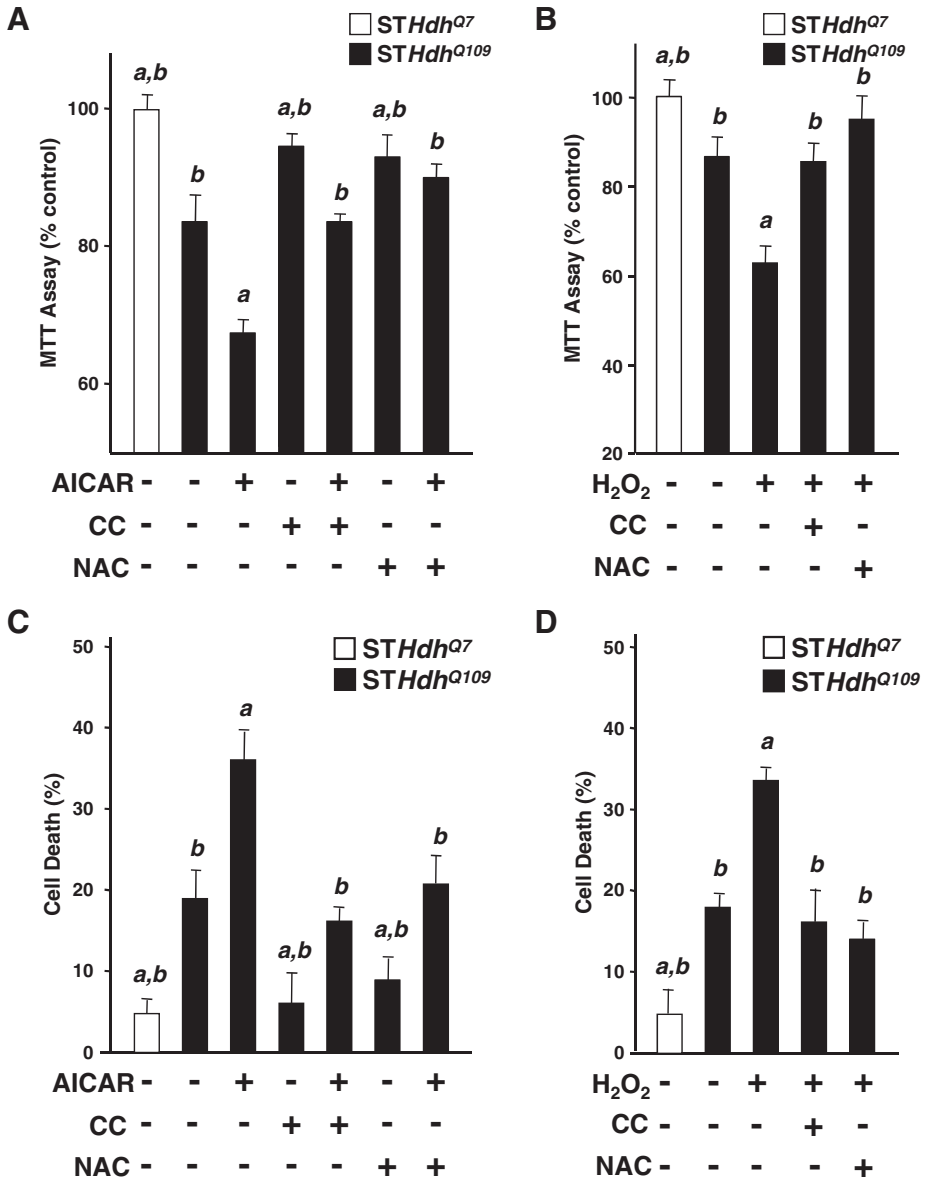

Fig. 7. A positive feedback regulation between reactive oxygen species (ROS) and AMPK promoted death of striatal cells. Cell survival was determined using the MTT assay (A, B) and a flow cytometric analysis (C, D). For the MTT assay, values of the indicated cells were normalized to those values of untreated ST*Hdh*^{Q7} cells. (A, C) Cells were treated with AICAR (1 mM), NAC (5 mM), and/or CC (10 μM) as indicated for 24 h. The data are presented as the mean ± SEM from three independent experiments. [a]$p < 0.05$ vs. untreated ST*Hdh*^{Q109} cells. [b]$p < 0.05$ vs. AICAR treated cells. (B, D) Cells were treated with H_2O_2 (100 μM), NAC (5 mM), and/or CC (10 μM) as indicated for 24 h. The data are presented as the mean ± SEM from three independent experiments. [a]$p < 0.05$ vs. untreated ST*Hdh*^{Q109} cells. [b]$p < 0.05$ vs. H_2O_2 treated cells.

blocks the impairment of contextual fear memory in a mouse model of AD [51]. It is believed that products of oxidative damage are usually harmful to normal cellular functions and, thus, worsen neurodegeneration. For example, 4-hydroxy-2-nonenal (4-HNE, a product of lipid peroxidation) suppresses the activity of the 26S proteasome [52] and, thus, might enhance the accumulation of disease-causing mutant proteins. Interestingly, the impairment of proteasomes further exacerbates the generation of oxidative stress [52], which suggests that feedback regulation between ROS and other harmful event(s) might be a common mechanism in neurodegeneration. In the present study, we demonstrated positive feedback regulation between ROS and AMPK-α1 in the striatum (Fig. 8). It is important to point out that, similar to what was observed in ST*Hdh*^{Q109} cells (Figs. 3 and 4) and primary striatal neurons (Fig. 5), a positive feedback regulation was found in primary cortical and hippocampal neurons (Fig. S4). An antioxidant (NAC) reduced the activation of AMPK, and an AMPK inhibitor (compound C, CC) suppressed the elevated ROS levels in both cortical and hippocampal neurons (Fig. S4). Thus, the positive feedback regulation between ROS and AMPK may also exist in many different types of neurons. Nonetheless, higher levels of ROS and AMPK activation were only found in the striatum of R6/2 mice (Fig. S5). Given that the striatum is particularly sensitive to oxidative stress [11,53], the feedback regulation between ROS and AMPK might occur mainly in the striatum under normal conditions, and may explain why the striatum is the most susceptible brain region in HD [54].

Our findings suggest that the positive regulation between ROS formation and AMPK-α1 during HD progression is likely to occur in the cytoplasm of striatal cells (Figs. 1, 5 and 8). The underlying mechanism for such regulation is largely uncharacterized. Earlier studies suggest that ROS may function upstream of AMPK through the activation of ATM or through the reduction of ATP content [55–57]. In addition, a recent report suggests that proline oxidase (POX) may mediate the regulation between ROS generation by AMPK in cancer cells. Given the importance of this vicious cycle in pathogenesis, further investigation concerning

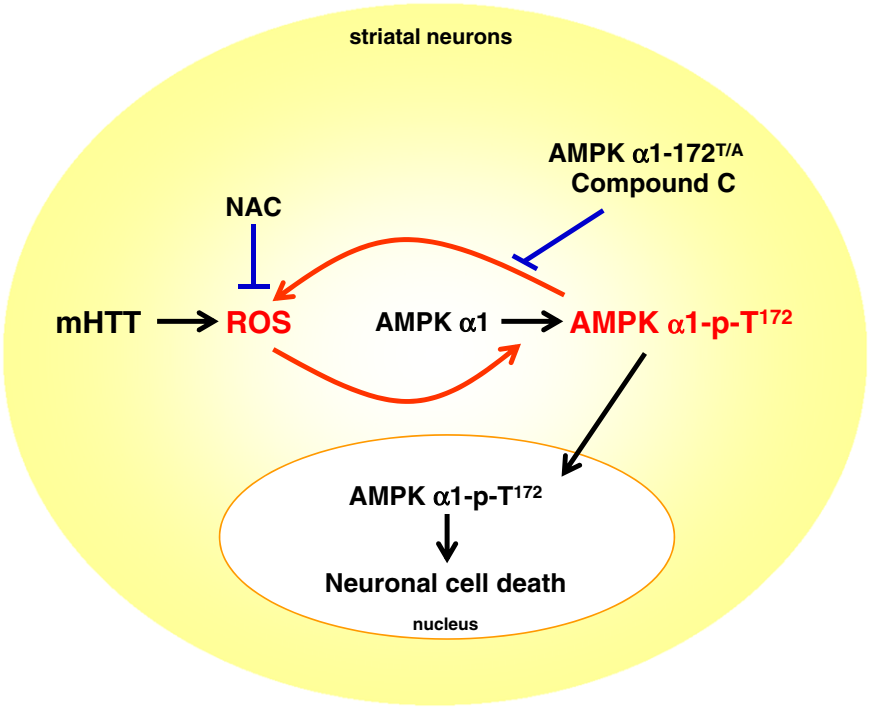

Fig. 8. A positive feedback regulation between reactive oxygen species (ROS) and AMPK activation contributes to HD progression. In the present study, we demonstrate that the expression of a polyQ-expanded mutant Huntingtin (mHTT) elevates cellular ROS in striatal cells or the striatum of a transgenic mouse model of HD (R6/2). Such increased ROS subsequently cause the abnormal activation of AMPK-α1. Conversely, the activation of AMPK-α1 induces the level of cellular ROS. A scavenger of ROS (i.e., *N*-acetyl-cysteine, NAC) and two inhibitors of AMPK-α1 (i.e., Compound C, AMPK-$\alpha1^{172T/A}$) reduce oxidative stresses, suppress AMPK activation, and protect striatal neurons. Collectively, the positive feedback regulation between AMPK-α1 and ROS contributes to neuronal atrophy during the progression of HD.

the molecular mechanism of this cycle is of great interest. Another critical aspect of such regulation is the isoform selectivity of AMPK. Our finding that elevated oxidative stress activates AMPK-α1 in striatal neurons during HD progression is consistent with previous findings in several other cell types (e.g., rat dental pulp cells, muscle, and NIH-3T3), in which AMPK-α1 mediates the action of ROS [26,58,59]. Nonetheless, in some other cell types (e.g., retinal pigment epithelium cell, glioma, and cardiomyocytes), AMPK-α2 (but not AMPK-α1) mediates the function of oxidative stress [41,60,61]. Although these two isoforms (AMPK α1 and α2) exhibit similar catalytic activity over an artificial substrate (SANS peptide) [62], many earlier studies suggested that AMPK-α1 and α2 are differentially regulated under different pathophysiological conditions. In patients with type 2 diabetes, acute exercise enhances the activity of AMPK-α2 (but not that of α1) in skeletal muscle and reduces the concentration of blood glucose [63]. In young non-diabetic humans, depletions of phosphocreatine and ATP levels lead to an increase of in AMPK-α2 activity in the muscle, with no significant change in that of AMPK-α1 [64]. It is most likely that AMPK-α1 and α2 play distinct roles in skeletal muscles during exercise. In addition to the differences in tissue distribution and subcellular localization, the substrate specificity of AMPK-α1 and α2 may also differ greatly [65]. Here, we report an important regulation of a detrimental AMPK-α1 in the striatum of HD mice by oxidative stress. Further investigations concerning the isoform-specific regulation of AMPK by ROS in the presence of mHTT may greatly advance our knowledge of the role of AMPK in neurodegenerative diseases.

5. Conclusions

In conclusion, we demonstrate that a vicious cycle of the elevated ROS and the activated AMPK-α1 in the striatum of HD mice contributes to the mHTT-induced neurotoxicity. The enhanced oxidative stress is an important upstream positive regulator of AMPK-α1, which promotes mHTT aggregation and worsens the mHTT-mediated neuronal atrophy. Chronic treatment of HD mice with a ROS scavenger (NAC) not only reduced the activation and nuclear enrichment of AMPK-α1, but also rescued the levels of a survival signal (Bcl2) that was impaired by AMPK-α1. Our findings suggest that ROS and AMPK-α1 are potential therapeutic targets for the treatment of HD.

Supplementary data to this article can be found online at http://dx.doi.org/10.1016/j.bbadis.2014.06.012.

Acknowledgements

We thank Drs. Elena Cattaneo and Marta Valenza for providing the striatal cell lines (ST*Hdh*^{Q109}, ST*Hdh*^{Q7}). This work was supported by grants from the National Science Council (NSC97-2321-B-001-030, NSC98-2321-B-001-017, NSC99-2321-B-001-012, and NSC100-2321-B-001-009) and Academia Sinica (AS-100-TP2-B02), Taiwan.

References

[1] T.H.s.D.C.R. Group, A novel gene containing a trinucleotide repeat that is expanded and unstable on Huntington's disease chromosomes. The Huntington's Disease Collaborative Research Group, Cell 72 (1993) 971–983.
[2] H. Li, S.H. Li, Z.X. Yu, P. Shelbourne, X.J. Li, Huntingtin aggregate-associated axonal degeneration is an early pathological event in Huntington's disease mice, J. Neurosci. 21 (2001) 8473–8481.
[3] G.J. Klapstein, R.S. Fisher, H. Zanjani, C. Cepeda, E.S. Jokel, M.F. Chesselet, M.S. Levine, Electrophysiological and morphological changes in striatal spiny neurons in R6/2 Huntington's disease transgenic mice, J. Neurophysiol. 86 (2001) 2667–2677.
[4] D. Martindale, A. Hackam, A. Wieczorek, L. Ellerby, C. Wellington, K. McCutcheon, R. Singaraja, P. Kazemi-Esfarjani, R. Devon, S.U. Kim, D.E. Bredesen, F. Tufaro, M.R. Hayden, Length of huntingtin and its polyglutamine tract influences localization and frequency of intracellular aggregates, Nat. Genet. 18 (1998) 150–154.
[5] J.P. Vonsattel, R.H. Myers, T.J. Stevens, R.J. Ferrante, E.D. Bird, E.P. Richardson Jr., Neuropathological classification of Huntington's disease, J. Neuropathol. Exp. Neurol. 44 (1985) 559–577.
[6] I.V. Kovtun, Y. Liu, M. Bjoras, A. Klungland, S.H. Wilson, C.T. McMurray, OGG1 initiates age-dependent CAG trinucleotide expansion in somatic cells, Nature 447 (2007) 447–452.
[7] A. Wyttenbach, O. Sauvageot, J. Carmichael, C. Diaz-Latoud, A.P. Arrigo, D.C. Rubinsztein, Heat shock protein 27 prevents cellular polyglutamine toxicity and

suppresses the increase of reactive oxygen species caused by huntingtin, Hum. Mol. Genet. 11 (2002) 1137–1151.
[8] W.J. Firdaus, A. Wyttenbach, P. Giuliano, C. Kretz-Remy, R.W. Currie, A.P. Arrigo, Huntingtin inclusion bodies are iron-dependent centers of oxidative events, FEBS J. 273 (2006) 5428–5441.
[9] F. Perez-Severiano, C. Rios, J. Segovia, Striatal oxidative damage parallels the expression of a neurological phenotype in mice transgenic for the mutation of Huntington's disease, Brain Res. 862 (2000) 234–237.
[10] A. Valencia, E. Sapp, J.S. Kimm, H. McClory, P.B. Reeves, J. Alexander, K.A. Ansong, N. Masso, M.P. Frosch, K.B. Kegel, X. Li, M. Difiglia, Elevated NADPH oxidase activity contributes to oxidative stress and cell death in Huntington's disease, Hum. Mol. Genet. 22 (2013) 1112–1131.
[11] M.B. Bogdanov, R.J. Ferrante, S. Kuemmerle, P. Klivenyi, M.F. Beal, Increased vulnerability to 3-nitropropionic acid in an animal model of Huntington's disease, J. Neurochem. 71 (1998) 2642–2644.
[12] P. Klivenyi, R.J. Ferrante, G. Gardian, S. Browne, P.E. Chabrier, M.F. Beal, Increased survival and neuroprotective effects of BN82451 in a transgenic mouse model of Huntington's disease, J. Neurochem. 86 (2003) 267–272.
[13] K.M. Smith, S. Matson, W.R. Matson, K. Cormier, S.J. Del Signore, S.W. Hagerty, E.C. Stack, H. Ryu, R.J. Ferrante, Dose ranging and efficacy study of high-dose coenzyme Q10 formulations in Huntington's disease mice, Biochim. Biophys. Acta 1762 (2006) 616–626.
[14] D.E. Ehrnhoefer, M. Duennwald, P. Markovic, J.L. Wacker, S. Engemann, M. Roark, J. Legleiter, J.L. Marsh, L.M. Thompson, S. Lindquist, P.J. Muchowski, E.E. Wanker, Green tea (−)-epigallocatechin-gallate modulates early events in huntingtin misfolding and reduces toxicity in Huntington's disease models, Hum. Mol. Genet. 15 (2006) 2743–2751.
[15] Y.C. Long, J.R. Zierath, AMP-activated protein kinase signaling in metabolic regulation, J. Clin. Invest. 116 (2006) 1776–1783.
[16] M.A. Raney, L.P. Turcotte, Evidence for the involvement of CaMKII and AMPK in Ca^{2+}-dependent signaling pathways regulating FA uptake and oxidation in contracting rodent muscle, J. Appl. Physiol. 104 (2008) 1366–1373.
[17] A. Woods, K. Dickerson, R. Heath, S.P. Hong, M. Momcilovic, S.R. Johnstone, M. Carlson, D. Carling, Ca^{2+}/calmodulin-dependent protein kinase kinase-beta acts upstream of AMP-activated protein kinase in mammalian cells, Cell Metab. 2 (2005) 21–33.
[18] A. Suzuki, G. Kusakai, A. Kishimoto, Y. Shimojo, T. Ogura, M.F. Lavin, H. Esumi, IGF-1 phosphorylates AMPK-alpha subunit in ATM-dependent and LKB1-independent manner, Biochem. Biophys. Res. Commun. 324 (2004) 986–992.
[19] M. Xie, D. Zhang, J.R. Dyck, Y. Li, H. Zhang, M. Morishima, D.L. Mann, G.E. Taffet, A. Baldini, D.S. Khoury, M.D. Schneider, A pivotal role for endogenous TGF-beta-activated kinase-1 in the LKB1/AMP-activated protein kinase energy-sensor pathway, Proc. Natl. Acad. Sci. U. S. A. 103 (2006) 17378–17383.
[20] R.L. Hurley, L.K. Barre, S.D. Wood, K.A. Anderson, B.E. Kemp, A.R. Means, L.A. Witters, Regulation of AMP-activated protein kinase by multisite phosphorylation in response to agents that elevate cellular cAMP, J. Biol. Chem. 281 (2006) 36662–36672.
[21] T.C. Ju, H.M. Chen, J.T. Lin, C.P. Chang, W.C. Chang, J.J. Kang, C.P. Sun, M.H. Tao, P.H. Tu, C. Chang, D.W. Dickson, Y. Chern, Nuclear translocation of AMPK-alpha1 potentiates striatal neurodegeneration in Huntington's disease, J. Cell Biol. 194 (2011) 209–227.
[22] Y. Minokoshi, T. Alquier, N. Furukawa, Y.B. Kim, A. Lee, B. Xue, J. Mu, F. Foufelle, P. Ferre, M.J. Birnbaum, B.J. Stuck, B.B. Kahn, AMP-kinase regulates food intake by responding to hormonal and nutrient signals in the hypothalamus, Nature 428 (2004) 569–574.
[23] J.S. Choi, C. Park, J.W. Jeong, AMP-activated protein kinase is activated in Parkinson's disease models mediated by 1-methyl-4-phenyl-1,2,3,6-tetrahydropyridine, Biochem. Biophys. Res. Commun. 391 (2010) 147–151.
[24] L.D. McCullough, Z. Zeng, H. Li, L.E. Landree, J. McFadden, G.V. Ronnett, Pharmacological inhibition of AMP-activated protein kinase provides neuroprotection in stroke, J. Biol. Chem. 280 (2005) 20493–20502.
[25] V. Vingtdeux, P. Davies, D.W. Dickson, P. Marambaud, AMPK is abnormally activated in tangle- and pre-tangle-bearing neurons in Alzheimer's disease and other tauopathies, Acta Neuropathol. 121 (2011) 337–349.
[26] T. Toyoda, T. Hayashi, L. Miyamoto, S. Yonemitsu, M. Nakano, S. Tanaka, K. Ebihara, H. Masuzaki, K. Hosoda, G. Inoue, A. Otaka, K. Sato, T. Fushiki, K. Nakao, Possible involvement of the alpha1 isoform of 5′AMP-activated protein kinase in oxidative stress-stimulated glucose transport in skeletal muscle, Am. J. Physiol. Endocrinol. Metab. 287 (2004) E166–E173.
[27] Y. Fukuyama, K. Ohta, R. Okoshi, H. Kizaki, K. Nakagawa, Hydrogen peroxide induces expression and activation of AMP-activated protein kinase in a dental pulp cell line, Int. Endod. J. 41 (2008) 197–203.
[28] J.E. Kim, Y.W. Kim, I.K. Lee, J.Y. Kim, Y.J. Kang, S.Y. Park, AMP-activated protein kinase activation by 5-aminoimidazole-4-carboxamide-1-beta-D-ribofuranoside (AICAR) inhibits palmitate-induced endothelial cell apoptosis through reactive oxygen species suppression, J. Pharmacol. Sci. 106 (2008) 394–403.
[29] G. Ceolotto, A. Gallo, I. Papparella, L. Franco, E. Murphy, E. Iori, E. Pagnin, G.P. Fadini, M. Albiero, A. Semplicini, A. Avogaro, Rosiglitazone reduces glucose-induced oxidative stress mediated by NAD(P)H oxidase via AMPK-dependent mechanism, Arterioscler. Thromb. Vasc. Biol. 27 (2007) 2627–2633.
[30] L. Mangiarini, K. Sathasivam, M. Seller, B. Cozens, A. Harper, C. Hetherington, M. Lawton, Y. Trottier, H. Lehrach, S.W. Davies, G.P. Bates, Exon 1 of the HD gene with an expanded CAG repeat is sufficient to cause a progressive neurological phenotype in transgenic mice, Cell 87 (1996) 493–506.
[31] C.H. Lin, S. Tallaksen-Greene, W.M. Chien, J.A. Cearley, W.S. Jackson, A.B. Crouse, S. Ren, X.J. Li, R.L. Albin, P.J. Detloff, Neurological abnormalities in a knock-in mouse model of Huntington's disease, Hum. Mol. Genet. 10 (2001) 137–144.
[32] E. Cattaneo, L. Conti, Generation and characterization of embryonic striatal conditionally immortalized ST14A cells, J. Neurosci. Res. 53 (1998) 223–234.
[33] C.D. Georgiou, I. Papapostolou, K. Grintzalis, Superoxide radical detection in cells, tissues, organisms (animals, plants, insects, microorganisms) and soils, Nat. Protoc. 3 (2008) 1679–1692.
[34] L. Riol-Blanco, C. Delgado-Martin, N. Sanchez-Sanchez, C.L. Alonso, M.D. Gutierrez-Lopez, G.M. Del Hoyo, J. Navarro, F. Sanchez-Madrid, C. Cabanas, P. Sanchez-Mateos, J.L. Rodriguez-Fernandez, Immunological synapse formation inhibits, via NF-kappaB and FOXO1, the apoptosis of dendritic cells, Nat. Immunol. 10 (2009) 753–760.
[35] A. Bouallegue, N.R. Pandey, A.K. Srivastava, CaMKII knockdown attenuates H2O2-induced phosphorylation of ERK1/2, PKB/Akt, and IGF-1R in vascular smooth muscle cells, Free Radic. Biol. Med. 47 (2009) 858–866.
[36] J. Palomeque, O.V. Rueda, L. Sapia, C.A. Valverde, M. Salas, M.V. Petroff, A. Mattiazzi, Angiotensin II-induced oxidative stress resets the Ca2+ dependence of Ca^{2+}-calmodulin protein kinase II and promotes a death pathway conserved across different species, Circ. Res. 105 (2009) 1204–1212.
[37] P.E. Chabrier, M. Auguet, Pharmacological properties of BN82451: a novel multitargeting neuroprotective agent, CNS Drug Rev. 13 (2007) 317–332.
[38] W.R. Galpern, M.E. Cudkowicz, Coenzyme Q treatment of neurodegenerative diseases of aging, Mitochondrion 7 (Suppl.) (2007) S146–S153.
[39] T.C. Ju, H.M. Chen, J.T. Lin, C.P. Chang, W.C. Chang, J.J. Kang, C.P. Sun, M.H. Tao, P.H. Tu, C. Chang, D.W. Dickson, Y. Chern, Nuclear translocation of AMPK-{alpha}1 potentiates striatal neurodegeneration in Huntington's disease, J. Cell Biol. 194 (2011) 209–227.
[40] Z. Hu, J. Chen, Q. Wei, Y. Xia, Bidirectional actions of hydrogen peroxide on endothelial nitric-oxide synthase phosphorylation and function: co-commitment and interplay of Akt and AMPK, J. Biol. Chem. 283 (2008) 25256–25263.
[41] K.M. Neurath, M.P. Keough, T. Mikkelsen, K.P. Claffey, AMP-dependent protein kinase alpha 2 isoform promotes hypoxia-induced VEGF expression in human glioblastoma, Glia 53 (2006) 733–743.
[42] I.J. Park, J.T. Hwang, Y.M. Kim, J. Ha, O.J. Park, Differential modulation of AMPK signaling pathways by low or high levels of exogenous reactive oxygen species in colon cancer cells, Ann. N. Y. Acad. Sci. 1091 (2006) 102–109.
[43] M. Gu, M.T. Gash, V.M. Mann, F. Javoy-Agid, J.M. Cooper, A.H. Schapira, Mitochondrial defect in Huntington's disease caudate nucleus, Ann. Neurol. 39 (1996) 385–389.
[44] M. Damiano, L. Galvan, N. Deglon, E. Brouillet, Mitochondria in Huntington's disease, Biochim. Biophys. Acta 1802 (2010) 52–61.
[45] F. Mochel, R.G. Haller, Energy deficit in Huntington disease: why it matters, J. Clin. Invest. 121 (2011) 493–499.
[46] A. Goswami, P. Dikshit, A. Mishra, S. Mulherkar, N. Nukina, N.R. Jana, Oxidative stress promotes mutant huntingtin aggregation and mutant huntingtin-dependent cell death by mimicking proteasomal malfunction, Biochem. Biophys. Res. Commun. 342 (2006) 184–190.
[47] C. Pimentel, L. Batista-Nascimento, C. Rodrigues-Pousada, R.A. Menezes, Oxidative stress in Alzheimer's and Parkinson's diseases: insights from the yeast Saccharomyces cerevisiae, Oxid. Med. Cell. Longev. 2012 (2012) 132146.
[48] S.C. Barber, P.J. Shaw, Oxidative stress in ALS: key role in motor neuron injury and therapeutic target, Free Radic. Biol. Med. 48 (2010) 629–641.
[49] P. Foley, P. Riederer, Influence of neurotoxins and oxidative stress on the onset and progression of Parkinson's disease, J. Neurol. 247 (Suppl. 2) (2000) II82–II94.
[50] C. Hureau, P. Faller, Abeta-mediated ROS production by Cu ions: structural insights, mechanisms and relevance to Alzheimer's disease, Biochimie 91 (2009) 1212–1217.
[51] Y.H. Hsiao, J.R. Kuo, S.H. Chen, P.W. Gean, Amelioration of social isolation-triggered onset of early Alzheimer's disease-related cognitive deficit by N-acetylcysteine in a transgenic mouse model, Neurobiol. Dis. 45 (2012) 1111–1120.
[52] P. Jenner, Oxidative stress in Parkinson's disease, Ann. Neurol. 53 (Suppl. 3) (2003) S26–S36 (discussion S36-28).
[53] A. Ferri, R. Duffard, A.M. de Duffard, Selective oxidative stress in brain areas of neonate rats exposed to 2,4-dichlorophenoxyacetic acid through mother's milk, Drug Chem. Toxicol. 30 (2007) 17–30.
[54] N.A. Aziz, D.F. Swaab, H. Pijl, R.A. Roos, Hypothalamic dysfunction and neuroendocrine and metabolic alterations in Huntington's disease: clinical consequences and therapeutic implications, Rev. Neurosci. 18 (2007) 223–251.
[55] A. Alexander, S.L. Cai, J. Kim, A. Nanez, M. Sahin, K.H. MacLean, K. Inoki, K.L. Guan, J. Shen, M.D. Person, D. Kusewitt, G.B. Mills, M.B. Kastan, C.L. Walker, ATM signals to TSC2 in the cytoplasm to regulate mTORC1 in response to ROS, Proc. Natl. Acad. Sci. U. S. A. 107 (2010) 4153–4158.
[56] I. Irrcher, V. Ljubicic, D.A. Hood, Interactions between ROS and AMP kinase activity in the regulation of PGC-1alpha transcription in skeletal muscle cells, Am. J. Physiol. Cell Physiol. 296 (2009) C116–C123.
[57] R.M. Mackenzie, I.P. Salt, W.H. Miller, A. Logan, H.A. Ibrahim, A. Degasperi, J.A. Dymott, C.A. Hamilton, M.P. Murphy, C. Delles, A.F. Dominiczak, Mitochondrial reactive oxygen species enhance AMP-activated protein kinase activation in the endothelium of patients with coronary artery disease and diabetes, Clin. Sci. (Lond.) 124 (2013) 403–411.
[58] Y. Fukuyama, K. Ohta, R. Okoshi, M. Suehara, H. Kizaki, K. Nakagawa, Hypoxia induces expression and activation of AMPK in rat dental pulp cells, J. Dent. Res. 86 (2007) 903–907.
[59] S.L. Choi, S.J. Kim, K.T. Lee, J. Kim, J. Mu, M.J. Birnbaum, S. Soo Kim, J. Ha, The regulation of AMP-activated protein kinase by H(2)O(2), Biochem. Biophys. Res. Commun. 287 (2001) 92–97.
[60] S. Qin, G.W. De Vries, Alpha2 but not alpha1 AMP-activated protein kinase mediates oxidative stress-induced inhibition of retinal pigment epithelium cell phagocytosis of photoreceptor outer segments, J. Biol. Chem. 283 (2008) 6744–6751.
[61] T. Horie, K. Ono, K. Nagao, H. Nishi, M. Kinoshita, T. Kawamura, H. Wada, A. Shimatsu, T. Kita, K. Hasegawa, Oxidative stress induces GLUT4 translocation by

activation of PI3-K/Akt and dual AMPK kinase in cardiac myocytes, J. Cell. Physiol. 215 (2008) 733–742.
[62] A. Woods, I. Salt, J. Scott, D.G. Hardie, D. Carling, The alpha1 and alpha2 isoforms of the AMP-activated protein kinase have similar activities in rat liver but exhibit differences in substrate specificity in vitro, FEBS Lett. 397 (1996) 347–351.
[63] N. Musi, N. Fujii, M.F. Hirshman, I. Ekberg, S. Froberg, O. Ljungqvist, A. Thorell, L.J. Goodyear, AMP-activated protein kinase (AMPK) is activated in muscle of subjects with type 2 diabetes during exercise, Diabetes 50 (2001) 921–927.
[64] N. Fujii, T. Hayashi, M.F. Hirshman, J.T. Smith, S.A. Habinowski, L. Kaijser, J. Mu, O. Ljungqvist, M.J. Birnbaum, L.A. Witters, A. Thorell, L.J. Goodyear, Exercise induces isoform-specific increase in 5′AMP-activated protein kinase activity in human skeletal muscle, Biochem. Biophys. Res. Commun. 273 (2000) 1150–1155.
[65] J. Weekes, K.L. Ball, F.B. Caudwell, D.G. Hardie, Specificity determinants for the AMP-activated protein kinase and its plant homologue analysed using synthetic peptides, FEBS Lett. 334 (1993) 335–339.